AIAA 80-0343R

Experiments on the Flow about a Supercritical Airfoil Including Holographic Interferometry

F. W. Spaid*
McDonnell Douglas Corporation, St. Louis, Mo.
and
W. D. Bachalo†
Spectron Development Laboratories, Inc., Costa Mesa, Calif.

Experiments were conducted on the transonic flow about a supercritical airfoil model, in which surface static and pitot pressure measurements were combined with data from holographic interferograms. The independent measurement of pitot pressure and density permits computing flowfield properties in the vicinity of the trailing edge and in the wake without recourse to static pressure assumptions. The data show significant static pressure gradients normal to the viscous layers in this region, extending approximately 10% chord downstream of the trailing edge. Comparisons are made between the experimental data and predictions from numerical computations.

Nomenclature

c = airfoil chord
C_l = airfoil section lift coefficient
C_p = pressure coefficient, $C_p = (P - P_\infty)/q_\infty$
$K_{G\text{-}D}$ = Gladstone-Dale constant
L_{eff} = effective optical path length
M = Mach number
P = pressure
q = dynamic pressure, $q = \frac{1}{2}\rho u^2$
Re_c = Reynolds number based on chord
u = velocity
x = coordinate measured parallel to freestream direction
z = distance from airfoil surface normal to x axis
α = angle of attack
α_{geom} = angle between the airfoil chordline and the test section centerline
δ^* = displacement thickness, $\delta^* = \int_0^\delta \left(1 - \frac{\rho u}{\rho_e u_e}\right) dz$
θ = momentum thickness, $\theta = \int_0^\delta \frac{\rho u}{\rho_e u_e}\left(1 - \frac{u}{u_e}\right) dz$
λ = laser wavelength
ρ = density

Subscripts
t = stagnation conditions
∞ = freestream conditions

Introduction

THE flowfield about a supercritical airfoil operating at its design Mach number and lift coefficient is characterized by regions of strong viscous-inviscid interaction, primarily the interaction of the upper-surface boundary layer with a shock wave and the trailing-edge region. The aft loading is associated with a large static pressure difference between the upper and lower surfaces just upstream of the trailing edge, remnants of which persist into the near wake. The coupling between the external inviscid flow and the viscous boundary layer and wake complicates the numerical computation of these flowfields. An inviscid computation of the flow about a more conventional airfoil often produces a static pressure distribution which is a good approximation to the experimental distribution, so that flowfield properties can be predicted adequately by iteration between an inviscid program and a boundary-layer program. Application of this procedure to an aft-loaded airfoil often fails, since the initial inviscid calculation is often so different from the actual flowfield that convergence to a physically realistic solution does not occur.

Numerous unpublished empirical fixes have been used to circumvent these difficulties in the computation of transonic flowfields about aft-loaded airfoils. Two examples are the addition of an estimated displacement thickness distribution to the airfoil coordinates prior to the initial inviscid calculation which is later replaced by results of boundary-layer calculations, and the extrapolation of the calculated boundary-layer displacement thickness distribution near the trailing edge in a manner which is known to facilitate agreement between the computed and experimental pressure distributions. A systematic, semiempirical method for the treatment of the trailing-edge region for both conventional and supercritical airfoils was proposed by Bavitz.[1] Results of a detailed analysis of the trailing-edge region were incorporated into a procedure for airfoil flowfield calculation developed by Melnik et al.[2] Analyses of the shock-wave/boundary-layer interaction region[3,4] have the potential for incorporation into an airfoil computation method. Several investigators[5-7] applied the Reynolds-averaged Navier-Stokes equations to the computation of airfoil flowfields.

The present study is one phase in a series of experiments on the flow about supercritical airfoils which is intended to provide data for comparison with the results of numerical computations. Surface static and pitot pressure measurements are combined with data from holographic interferograms, resulting in an unusually complete description of the time-mean flowfields.

Facilities and Instrumentation

The experiments were part of a cooperative program between McDonnell Douglas Research Laboratories (MDRL) and the NASA Ames Research Center. They were conducted in the Two-by-Two-Foot Transonic Wind Tunnel of the Ames Research Center, as modified for two-dimensional testing. A 15.24 cm chord model of essentially the original NASA Whitcomb integral (unslotted) supercritical airfoil section was

Presented as Paper 80-0343 at the AIAA 18th Aerospace Sciences Meeting, Pasadena, Calif., Jan. 14-16, 1980; submitted April 11, 1980; revision received July 28, 1980.

*Senior Scientist, McDonnell Douglas Research Laboratories. Associate Fellow AIAA.
†Senior Scientist. Member AIAA.

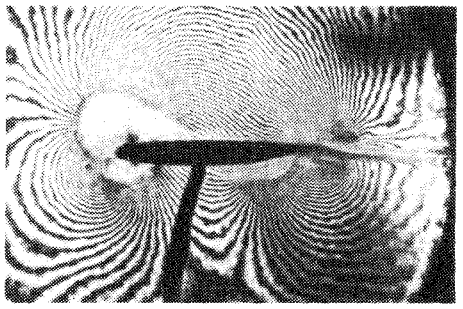
a)

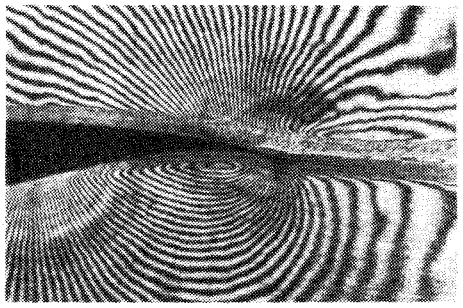
b)

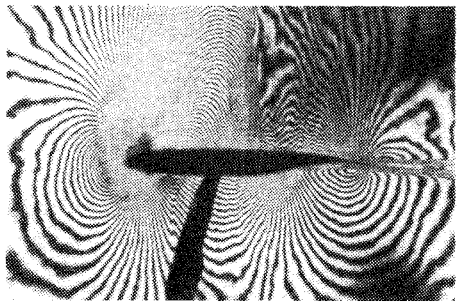
c)

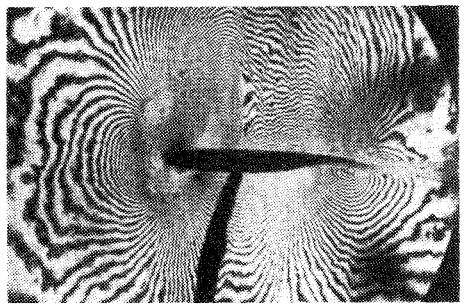
d)

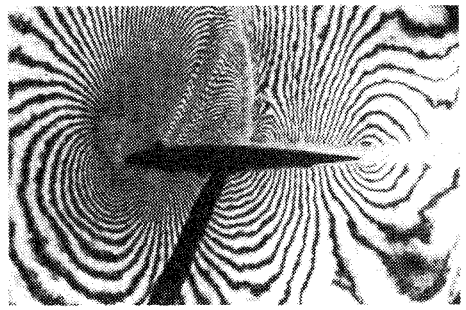
e)

Fig. 1 Interferograms of transonic airfoil flowfields. a) Supercritical airfoil, $M_\infty = 0.6$, $Re_c = 4 \times 10^6$, $C_l = 0.58$; b) supercritical airfoil $M_\infty = 0.6$, $Re_c = 4 \times 10^6$, $C_l = 0.58$, closeup of trailing edge region; c) supercritical airfoil, $M_\infty = 0.8$, $Re_c = 2 \times 10^6$, $C_l = 0.61$; d) supercritical airfoil, $M_\infty = 0.8$, $Re_c = 3 \times 10^6$, $C_l = 0.44$; e) NACA 64A010 airfoil, $M_\infty = 0.8$, $Re_c = 2 \times 10^6$, $C_l = 0.50$.

mounted between rotating optical glass windows in the solid, plane sidewalls. Pitot pressure surveys were made with a two degrees-of-freedom traversing rig and probe assembly mounted on the tunnel sting. This assembly allowed remote streamwise and vertical movement of the probe, which has a tip thickness of 0.10 mm. Holographic interferograms were obtained with a system which utilized the existing tunnel Schlieren mirrors, a pulsed ruby laser for creating the holograms, and helium-neon laser for hologram reconstruction. Holograms were obtained showing the entire field of view of the test section windows, both with and without flow in the test section. After processing, the no-flow plate and one of the plates taken at test conditions were positioned in a reconstruction plate holder, illuminated with the reference beam, and aligned for infinite-fringe interferograms. This dual-plate method[8] allows the fringe orientation to be chosen during reconstruction. Since the method involves interference between waves that follow the same optical path but are separated in time, imperfections in optical elements are cancelled.

A disadvantage of the dual-plate method can cause difficulty if the field of view does not include a region of uniform flow, which causes wavefronts throughout the field of view to be distorted by density gradients. In that case, there is no direct means to verify that the system is in the alignment required for infinite-fringe interferometry.

If the flow is adequately two-dimensional, fringes on an infinite-fringe interferogram correspond to density contours in the flow, with a constant density increment between fringes given by

$$\rho_1 - \rho_2 = \frac{\lambda}{L_{\text{eff}} K_{\text{G-D}}}$$

where ρ_1 and ρ_2 are the densities at two adjacent fringes, L_{eff} is the effective optical path length including the effect of the sidewall boundary layers, λ is the laser wavelength, and $K_{\text{G-D}}$ is the Gladstone-Dale constant. The value of density at one fringe must be determined by independent means. The method used in this investigation was to choose the density level at a reference fringe to give the best overall agreement between surface static pressures derived from interferograms and those measured at static pressure orifices.

More detailed information concerning the holography system can be found in Ref. 9. Descriptions of the facility, the traversing rig and probe, and coordinates of the model are contained in Refs. 10-12.

Results and Discussion

Interferograms

Examples of interferograms are presented in Fig. 1. Values of angle of attack are not given because an adequate method for correcting the angle of attack for wall interference effects has not yet been developed for this test section. Figure 1a shows a predominantly subcritical case. A close-up of the trailing-edge region is shown in Fig. 1b. Boundary-layer transition strips for the case shown in Figs. 1a and 1b were located at $x/c = 0.05$ on the upper surface and $x/c = 0.18$ on the lower surface. The recommendations of Braslow et al.[13] were used as guidelines in selecting trip configurations. Two supercritical cases with upper-surface shocks corresponding to two different angles of attack are shown in Figs. 1c and 1d. For these test conditions, the boundary-layer trips were located at $x/c = 0.35$ on the upper surface and $x/c = 0.18$ on the lower surface. An interferogram for the uncambered NACA 64A010 airfoil from Ref. 9 is included in Fig. 1e for comparison. Fringe patterns in the viscous and inviscid regions are distinctly different. As a result, the approximate boundaries of the viscous regions are visible. Within the viscous regions, the static pressure varies only in the streamwise direction, except near the shock and the trailing

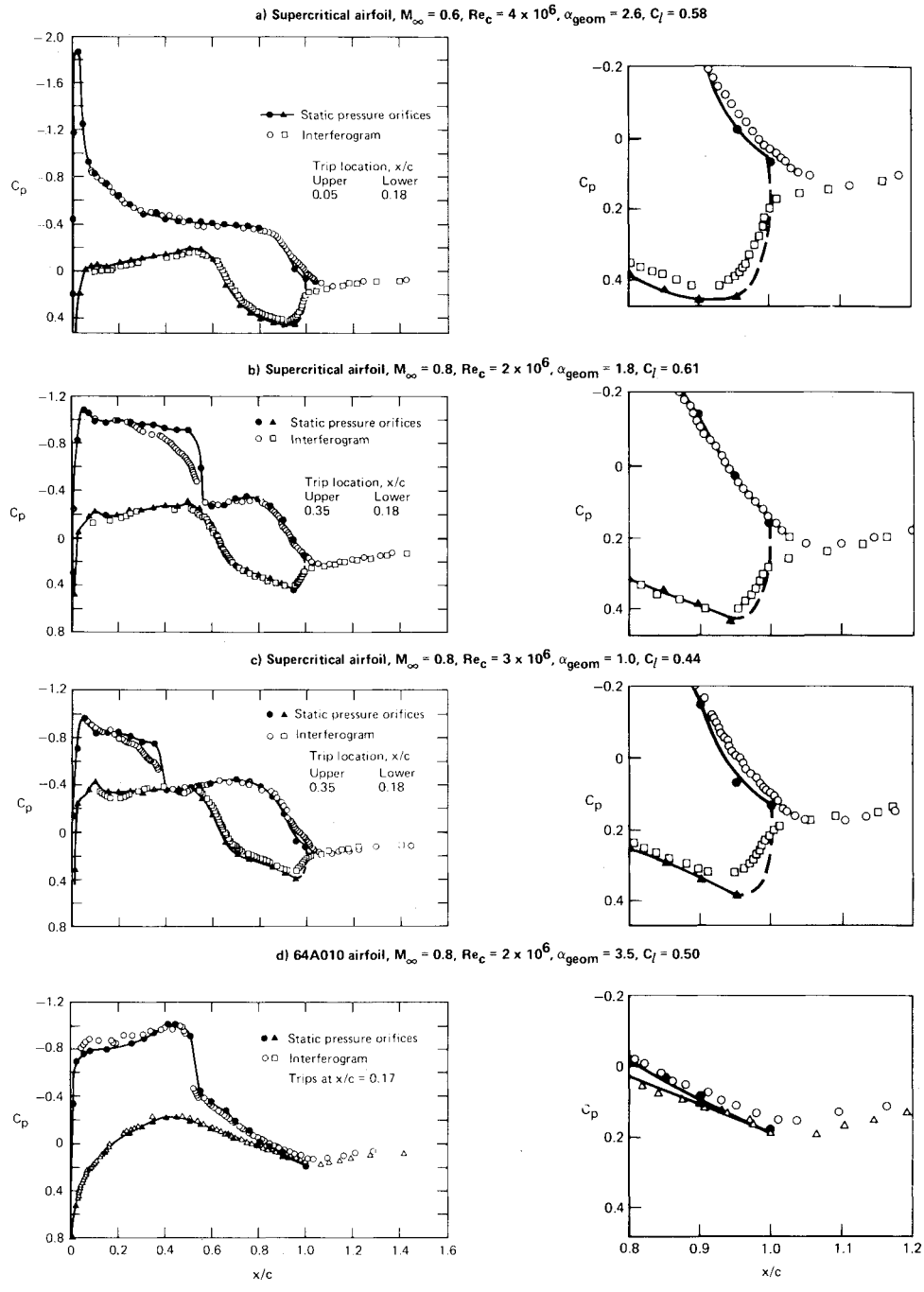

Fig. 2 Comparison of data from static pressure orifices and pressures determined from interferograms.

edge, but the fringe patterns show density gradients to be approximately parallel to the streamlines. Static temperature variations associated with adiabatic deceleration must therefore be the predominant mechanism for production of density variations in the boundary layers and wakes. Differences in the fringe patterns between the two airfoils near the trailing edge result from the stronger viscous interaction in this region associated with the supercritical airfoil. The closed contours in the primarily inviscid flow are located symmetrically above and below the trailing edge. By contrast, the closed contours are displaced streamwise in the interferograms corresponding to the supercritical airfoil, indicating local maxima of density both in the lower-surface concavity and downstream of the trailing edge on the upper surface of the near wake. The fringe pattern in the lower-surface boundary layer near the trailing edge is a composite of the viscous and inviscid patterns, indicating that adiabatic deceleration and static pressure gradients are of comparable importance in producing variations in this region.

Static Pressure Data

Data from static pressure orifices and pressures determined from the interferograms using the assumption of constant stagnation pressure and stagnation temperature are compared in Fig. 2. Pitot pressure data obtained for the test conditions of Fig. 2b show the stagnation pressure at the boundary-layer edge downstream of the shock to be equal to the freestream value within experimental uncertainty. As a result, no corrections for shock losses were made in the computation of static pressure from interferogram data. Agreement is generally good between the two types of data, implying that a close approximation to infinite-fringe alignment was achieved. Oil-flow visualization photographs obtained from an unpublished phase of this cooperative program show that upper-surface shocks on the supercritical airfoil sweep forward near the side walls, causing an apparent smearing of the shock compression in the interferogram data. The comparison of Fig. 2d for the 64A010 airfoil indicates that the flow near the shock is more nearly two-dimensional. Ap-

parently the greater upper-surface curvature of this airfoil causes the shock to remain at a more nearly constant chordwise location than it does on the supercritical section.

The interferogram data give static pressure distributions at the edges of the boundary layer and near wake which are difficult to measure by other techniques. Significant static pressure gradients normal to streamlines are present in the near-wake data for the supercritical airfoil, extending approximately 10% chord downstream in Figs. 2a and 2b. The effect is less pronounced in Fig. 2c and for the conventional airfoil. Pressure variations across the lower-surface boundary layer near the trailing edge are present in the data for the supercritical airfoil. The flow is known to be attached[12] in the lower-surface concavity at the test conditions of Fig. 2a, $M_\infty = 0.6$; the static pressure varies across the boundary layer throughout most of the lower-surface concavity in this situation. On the other hand, little or no static pressure variation normal to the surface is indicated in the data of Fig. 2b for $M_\infty = 0.8$, $C_l = 0.61$, where the flow was separated in the concavity. The flow in the concavity at $M_\infty = 0.8$, $C_l = 0.44$ was also separated, and the comparison of Fig. 2c also indicates little static pressure variation across the separated boundary layer.

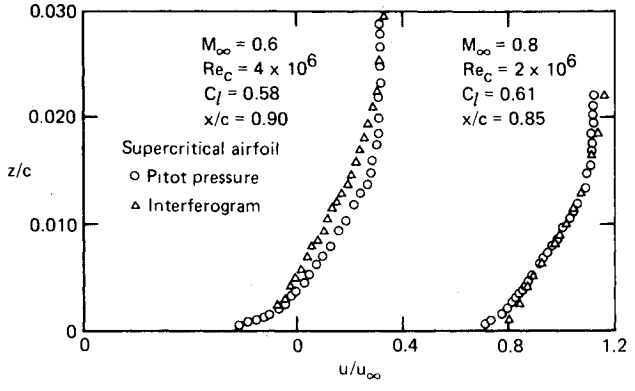

Fig. 3 Comparison of upper-surface boundary-layer profiles derived from pitot pressure measurements and from interferograms.

Viscous Flow Profiles

Figure 3 presents boundary-layer profiles derived independently from pitot pressure and interferometry data. These data were reduced employing the usual assumption that the static pressure does not vary in the direction normal to the surface. This comparison serves primarily as a check on both types of data since the techniques are subject to different error sources, and as demonstration of repeatability since the data were obtained during different tunnel entries. Other comparisons of this type show similar trends; the profiles obtained by the two methods at $M_\infty = 0.8$ were always in better agreement than those obtained at $M_\infty = 0.6$.

Trailing-edge profiles of density, pitot pressure, velocity, and static pressure are presented in Fig. 4. The velocity and static pressure data were derived from the density and pitot pressure measurements, with the assumption of constant stagnation temperature. Integral properties for these profiles were calculated as described in Ref. 11, with the modifications for static pressure variation across the boundary layers proposed by Zwaaneveld.[14] These data show a decreasing static pressure level with increasing z/c. A major portion of the waviness in the derived C_p distributions is undoubtedly associated with the fact that the density and pitot pressure

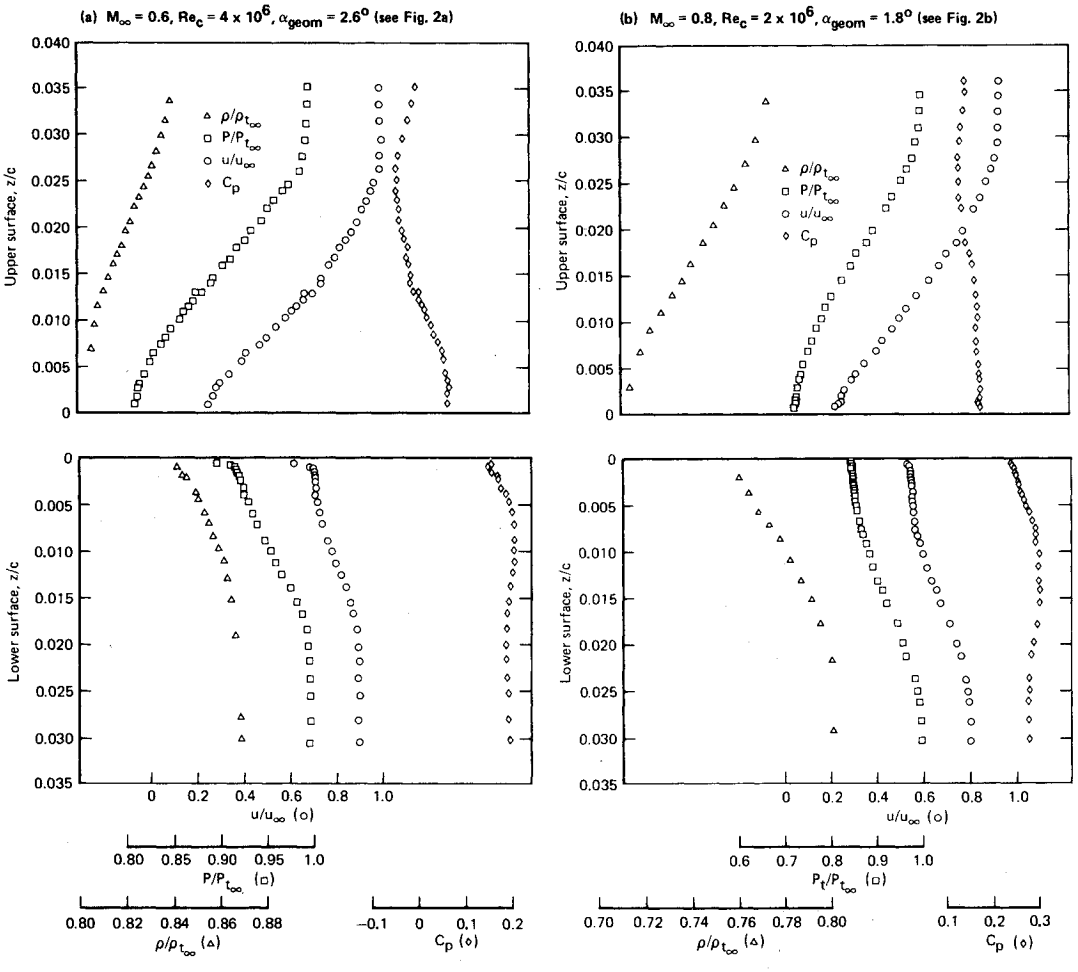

Fig. 4 Trailing-edge boundary-layer profiles derived from pitot pressure and interferogram data, supercritical airfoil.

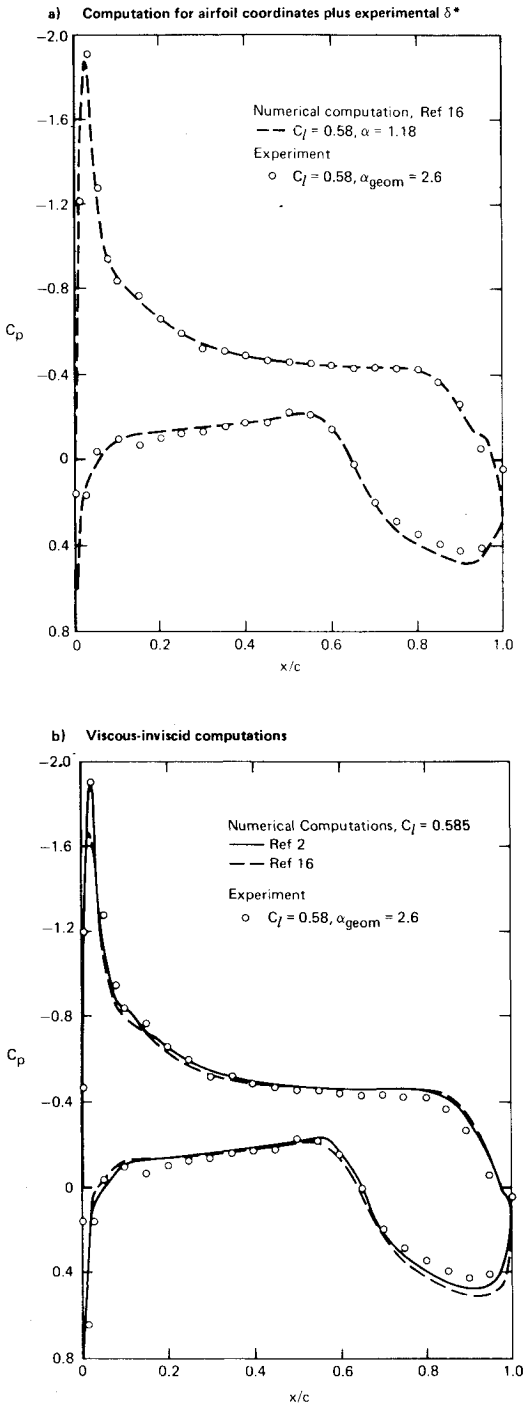

Fig. 5 Calculated static pressure distribution compared with experiment, $M_\infty = 0.6$, $Re_c = 4 \times 10^6$ (see Fig. 2a).

data were obtained in separate experiments. Errors in the location of the z-axis origin relative to the measured profiles may also have contributed to errors in calculated static pressure. These data show a static pressure variation throughout the upper-surface boundary layer. Most of the variations in C_p within the lower-surface profiles are confined to the region near the surface. The average C_p levels in the lower-surface profiles are significantly higher than the trailing-edge surface C_p's. The surface measurements were made with aft-facing orifices in the trailing edge, a technique which would be expected to give an average static pressure level for the entire trailing-edge region.

The use of the surface trailing-edge C_p in computing velocities and integral properties for the lower-surface trailing-edge boundary layers leads to large errors. The lower-surface trailing-edge velocities of Ref. 12 were computed using the present method for the cases where interferograms were available; C_p increments between the trailing-edge static pressure orifice and the average value for the lower-surface profile derived from the present study were used for the remaining cases.

Comparisons with Computations

Comparisons between measured and computed static pressure distributions are presented in Fig. 5 for the test condition at $M_\infty = 0.6$. The computation technique, developed by Garabedian and Korn[15] and extended by Tranen,[16] uses the full-potential equation for two-dimensional, inviscid transonic flow in conjunction with a quasiconservative, rotated differencing scheme. The effective airfoil shape used for the calculation of Fig. 5a was obtained by adding a displacement thickness distribution faired through the measured values for this case[12] to the airfoil coordinates, resulting in a profile having an open trailing edge. When transformed to the physical plane, the computed flowfield includes a source within the airfoil, having a strength determined by the trailing-edge thickness. Agreement between the experimental and computed distribution is generally good, although the measured C_p levels were shifted by -0.03 for this comparison. Discrepancies on the lower surface near the leading edge are believed to be caused by deviations of the airfoil model contour from the prescribed coordinates. Pressure levels in the concavity are strongly affected by the displacement thickness distribution. Since the experimental values are used here, the difference between the measured and computed static pressure distribution in this region is greater than expected. Static pressure levels in the concavity derived from the interferogram are even lower than the pressure orifice data of Fig. 5a.

The experimental data of Fig. 2a are compared with predictions of viscous-inviscid computations in Fig. 5b. The method of Ref. 16 is a conventional iteration between inviscid and boundary-layer computation procedures, employing extrapolation of the computed displacement thickness distribution near the trailing edge for $x/c > 0.997$. The method proposed by Melnik et al.[2] includes a detailed treatment of the trailing-edge and near-wake flowfield. In both cases the computed aft loading is greater than that shown by the data.

Momentum and displacement thickness distributions for the boundary layers and the near wake obtained from the computations of Fig. 5b are compared with experimental data in Fig. 6. The comparison for the upper-surface boundary layer is given in Fig. 6a. Both of the computed boundary-layer thickness distributions lie somewhat below the data, particularly for $x/c > 0.9$. Considerably better agreement would have been obtained if the computed shape factor δ^*/θ were closer to the measured value at $x/c \cong 0.8$, approximately at the beginning of the region of adverse pressure gradient. The computed response of a turbulent boundary layer to an adverse pressure gradient is sensitive to upstream conditions, particularly if the initial shape factor is greater than that corresponding to zero static pressure gradient. Better agreement between the experimental lower-surface boundary-layer properties and the predictions of Ref. 2 is shown in Fig. 6b. Since the special treatment of the trailing-edge region extends upstream for a distance of the order of a boundary-layer thickness, differences in computed boundary-layer properties shown in Fig. 6b are probably the result of differences in the boundary-layer computation methods. The computed static pressure distributions differ from the experimental distribution in the concavity. Boundary-layer computations using the experimental static pressure distribution would result in significantly smaller computed displacement thicknesses in the concavity than the distributions of Fig. 6b.

Near-wake displacement and momentum thicknesses computed by the method of Melnik et al.[2] for the $M_\infty = 0.6$ case are in good agreement with experimental data, as shown

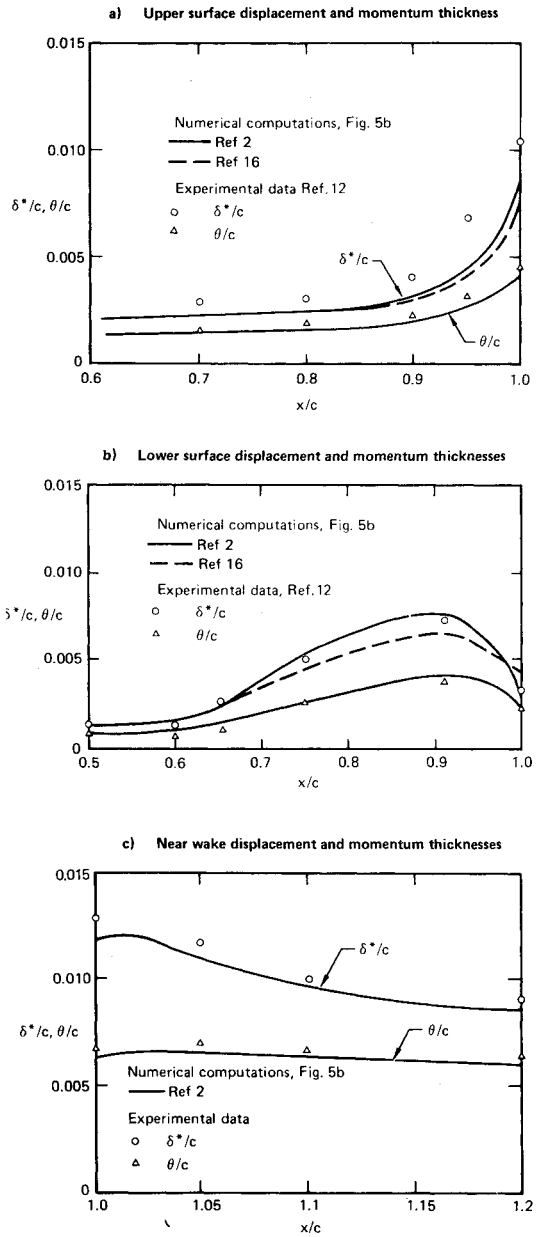

Fig. 6 Comparison of calculated and measured boundary-layer and wake properties, $M_\infty = 0.6$, $Re_c = 4 \times 10^6$, $C_l = 0.61$.

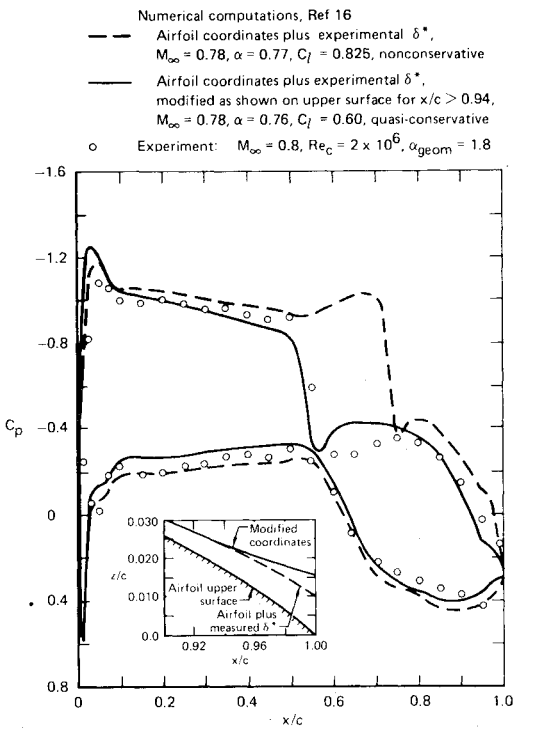

Fig. 7 Comparison of calculated and measured static pressure distributions.

in Fig. 6c. Comparisons of wake velocity profiles similar to those presented in Fig. 3 for boundary-layer data, in which the interferogram and pitot pressure data were reduced independently, show reasonable agreement except near the wake centerline where the minimum velocities derived from the interferograms are greater than those computed from the pitot pressure measurements. Although the cause of this discrepancy is not completely understood, the fact that the interferogram represents an average of the density field over the test section width is believed to be a contributing factor. The pitot and static pressure data are time-averaged measurements, but the holograms from which the interferograms were made are essentially instantaneous measurements since the laser pulse duration was approximately 20 ns. This difference may also be responsible for some of the discrepancies between the two types of data. Near-wake velocities were computed from the pitot pressure data, using static pressure levels determined from the interferogram at the edges of the wake and assuming a linear variation in static pressure across the wake. The interferograms show that elevated static pressure levels persist relatively far downstream of the trailing edge. Since momentum and displacement thicknesses determined from pitot pressure surveys are relatively sensitive to the static pressure used in data reduction, interferometry is valuable in obtaining an accurate description of this type of wake.

Comparisons between the experimental static pressure distribution and static pressure distributions computed by the method of Ref. 16 for the supercritical case shown in Fig. 1c are presented in Fig. 7. Inviscid computations were performed for an effective airfoil shape obtained by adding a displacement thickness distribution faired through the measured values. The dashed line represents results of a nonconservative calculation performed at $M_\infty = 0.78$, with the angle of attack chosen to give reasonable agreement with the static pressure levels on the forward portion of the airfoil. Similar calculations performed at higher Mach number and those performed using quasiconservative differencing tended to form strong shocks near the trailing edge and failed to converge. Viscous-inviscid calculations using the method of Ref. 2 were similarly unsuccessful. The inverse feature developed by Tranen[16] was used to determine an effective airfoil shape which would yield approximately the experimental pressure distribution. The result is indicated by the solid line, also computed for $M_\infty = 0.78$ but using quasiconservative differencing. The required modification to the effective airfoil shape is shown in the insert, consisting of an upward deflection of the upper surface, beginning at $x/c = 0.94$ and corresponding to a displacement thickness 50% greater than the measured value at the trailing edge. Preliminary calculations in which the effective airfoil shape was extended downstream of the trailing edge using a fairing of the measured displacement thickness distribution gave similar results; the initial analysis calculation leads to shock waves which are too strong and too far aft, and unreasonably large wake displacement thickness distributions are required to move the shock forward.

Additional comparisons between measured and computed results are presented in Fig. 8 in the form of Mach number contours. The edges of the boundary layers and wakes obtained from the interferograms are also shown. Agreement between measured and computed contours is reasonably good near the airfoil, and becomes poorer with increasing distance

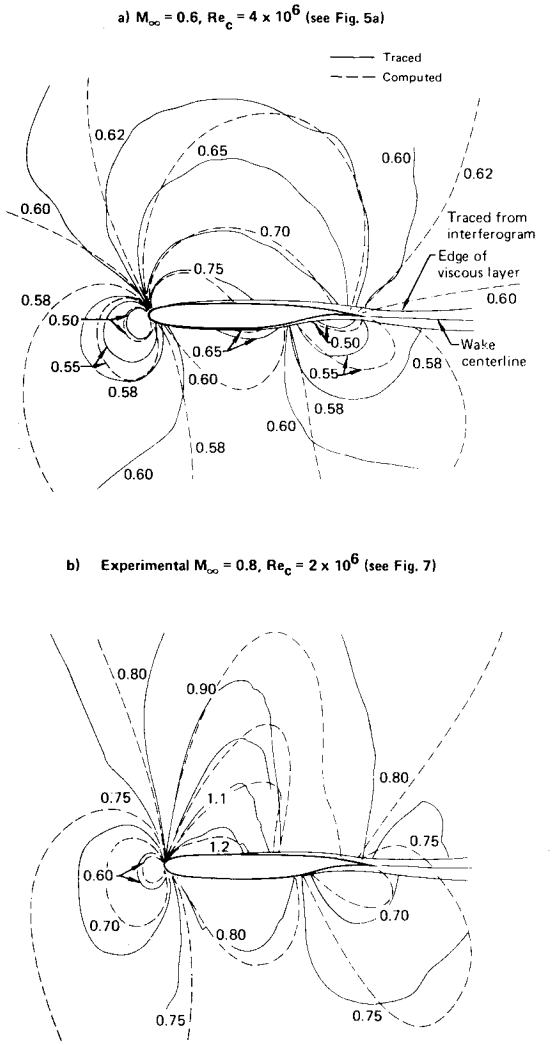

Fig. 8 Comparison of Mach number contours traced from interferogram with computed contours.

from the airfoil. The experimental contours show a more rapid approach to freestream conditions with distance from the airfoil, normal to the chord line, than the computed contours. If the behavior of the computed contours at some distance from the airfoil is representative of flow in an unbounded medium, then the behavior of the measured contours implies a situation more like that of flow in a free jet. In a free-jet flow, a constant static pressure level is imposed at the jet boundary, thereby forcing the disturbance field produced by the airfoil to vanish more rapidly with distance from the airfoil than it would in free air. Interpretation of the comparison of Fig. 8b is complicated because the computation was performed at $M_\infty = 0.78$, but Mach numbers assigned to the fringes were determined assuming $M_\infty = 0.8$. Alternate methods of comparison, such as assuming the experimental M_∞ to be lower or selecting experimental fringes to match the density ratio of the computed contours, resulted in poorer agreement than that shown in Fig. 8b.

It is also possible that the interferometer was not set exactly in the infinite-fringe mode. As discussed previously, there was no means available to verify that the setting was in infinite-fringe mode when the wavefronts in the entire field of view were disturbed by the flow about the airfoil. A method has since been devised to eliminate this difficulty in future investigations.

Comparisons between measured and calculated density contours, using data obtained from the same wind tunnel, were presented by Rose and Seginer.[6] These comparisons imply that the effective angle of attack in the tunnel is a function of streamwise location. This conclusion is based in part on discrepancies between computed and measured contours upstream of the leading edge, in which the angle of attack of the computation was chosen to give best overall agreement with the experimental surface static pressures. The trend of disagreement between measured and computed contours for that comparison is the reverse of that shown in Fig. 8. In the comparison of Ref. 6, the computed contours approach the freestream conditions more rapidly than the experimental contours with increasing distance upstream of the leading edge. The experimental contours approach the freestream conditions more rapidly than the computed contours with distance normal to the chord line in the comparisons of Ref. 6, a trend which is consistent with the present results.

Conclusion

Data were obtained on the flow about a supercritical airfoil, including pitot pressure surveys in the viscous regions and holographic interferograms. Combination of surface static pressures, pitot pressures, and interferogram data provides detailed descriptions of time-mean flowfields about this airfoil. The average static pressure level in the lower-surface boundary layer at the trailing edge is substantially higher than the pressure measured by the trailing-edge orifice.

Static pressure gradients normal to the wake extend approximately 10% chord downstream of the trailing edge. Computations of the surface static pressure distribution, employing both measured and calculated displacement thickness distributions are in reasonable agreement with experiment at $M_\infty = 0.6$. Good agreement between measured lower-surface boundary layer and near-wake properties and predictions of a viscous-inviscid interaction method is shown at $M_\infty = 0.6$. Growth of the upper-surface boundary layer near the trailing edge is underpredicted for that case. Reasonable agreement between a measured static pressure distribution and one computed by an inviscid transonic computer program for a case at $M_\infty = 0.8$ characterized by an upper-surface shock at midchord requires a reduction in the Mach number of the computation to 0.78 and modification of the effective upper-surface contour near the trailing edge, equivalent to adding a trailing-edge displacement-thickness 50% greater than the experimental value. Comparisons of computed Mach number contours with contours derived from interferograms show differences which could be interpreted as wall interference effects.

Acknowledgments

This research was conducted under the McDonnell Douglas Independent Research and Development Program in cooperation with the NASA Ames Research Center. Part of this investigation was performed by Spectron Development Laboratories, Inc., under contract to McDonnell Douglas Corporation.

References

[1] Bavitz, P. C., "An Analysis Method for Two-Dimensional Transonic Viscous Flow," NASA TN D-7718, Jan. 1975.

[2] Melnik, R. E., Chow, R., and Mead, H. R., "Theory of Viscous Transonic Flow Over Airfoils at High Reynolds Number," AIAA Paper 77-680, Albuquerque, New Mex., June 27-29, 1977.

[3] Inger, G. R. and Mason, W. H., "Analytical Theory of Transonic Normal Shock-Boundary Layer Interaction," *AIAA Journal,* Vol. 14, Sept. 1976, pp. 1266-1272.

[4] Bohning, R. and Zierep, J., "Condition for the Onset of Separation of the Turbulent Boundary Layer on a Curved Wall with a Normal Shock Wave," translated from *Zeitschrift fur angewandte Mathematik and Physik,* Vol. 29, 1978.

[5] Deiwert, G. S., "Numerical Simulation of High Reynolds Number Transonic Flows," *AIAA Journal,* Vol. 13, Oct. 1975, pp. 1354-1359.

[6]Rose, W. C. and Seginer, A., "Calculation of Transonic Flow Over Supercritical Airfoil Sections," AIAA Paper 77-681, Albuquerque, New Mex., June 27-29, 1977.

[7]Walitt, L., King, L. S., and Liu, C. Y., "Computation of Viscous Transonic Flow About a Lifting Airfoil," AIAA Paper 77-679, Albuquerque, New Mex., June 27-29, 1977.

[8]Trolinger, J. D., "Laser Instrumentation for Flow Field Diagnostics," AGARDograph 186, 1974.

[9]Johnson, D. A. and Bachalo, W. D., "Transonic Flow About a Two-Dimensional Airfoil – Inviscid and Turbulent Flow Properties," AIAA Paper 78-1117, Seattle, Wash., July 10-12, 1978.

[10]Hurley, F. X., Spaid, F. W., Roos, F. W., Stivers, L. S. Jr., and Bandettini, A., "Detailed Transonic Flow Field Measurements about a Supercritical Airfoil Section," NASA TM X-3244, July 1975.

[11]Hurley, F. X., Spaid, F. W., Roos, F. W., Stivers, L. S. Jr., and Bandettini, A., "Supercritical Airfoil Flowfield Measurements," *Journal of Aircraft,* Vol. 12, Sept. 1975, pp. 737-744.

[12]Spaid, F. W. and Stivers, L. S. Jr., "Supercritical Airfoil Boundary Layer Measurements," AIAA Paper 79-1501, Williamsburg, Va., July 23-25, 1979.

[13]Braslow, A. L., Hicks, R. M., and Harris, R. V. Jr., "Use of Grit-Type Boundary-Layer-Transition Trips on Wind-Tunnel Models," NASA TN D-3579, Sept. 1966.

[14]Zwaaneveld, J., "Comparison of Various Methods for Calculating Profile Drag from Pressure Measurements in the Near Wake at Subcritical Speeds," *Aerodynamic Drag,* AGARD Conference Proceedings 124, 1973.

[15]Garabedian, P. R. and Korn, D. G., "Analysis of Transonic Airfoils," *Communications on Pure and Applied Mathematics,* Vol. 24, 1971, p. 841.

[16]Tranen, T. L., "A Rapid Computer Aided Transonic Airfoil Design Method," AIAA Paper 74-501, Palo Alto, Calif., June 17-19, 1974.